This is a repository copy of *FAST-forge − a new cost-effective hybrid processing route for consolidating titanium powder into near net shape forged components*.

White Rose Research Online URL for this paper:
https://eprints.whiterose.ac.uk/id/eprint/147740/

Version: Accepted Version

Article:
Weston, N.S. orcid.org/0000-0002-0515-4573 and Jackson, M. (2017) FAST-forge − a new cost-effective hybrid processing route for consolidating titanium powder into near net shape forged components. Journal of Materials Processing Technology, 243. pp. 335-346. ISSN 0924-0136

https://doi.org/10.1016/j.jmatprotec.2016.12.013

Article available under the terms of the CC-BY-NC-ND licence (https://creativecommons.org/licenses/by-nc-nd/4.0/).

Reuse
This article is distributed under the terms of the Creative Commons Attribution-NonCommercial-NoDerivs (CC BY-NC-ND) licence. This licence only allows you to download this work and share it with others as long as you credit the authors, but you can't change the article in any way or use it commercially. More information and the full terms of the licence here: https://creativecommons.org/licenses/

Takedown
If you consider content in White Rose Research Online to be in breach of UK law, please notify us by emailing eprints@whiterose.ac.uk including the URL of the record and the reason for the withdrawal request.

eprints@whiterose.ac.uk
https://eprints.whiterose.ac.uk/

FAST-*forge* – a new cost-effective hybrid processing route for consolidating titanium powder into near net shape forged components

N. S. Weston*[a], M. Jackson[a]

[a]The University of Sheffield, Department of Materials Science and Engineering, Sir Robert Hadfield Building, Mappin Street, Sheffield, S1 3JD, United Kingdom.

*Corresponding author email: n.weston@sheffield.ac.uk

Abstract

Reducing the high cost of titanium to a level where it can compete with currently used commodity metals offers opportunities to many industries to exploit its excellent combination of properties to improve performance or reduce weight. The key to decreasing cost is to reduce the number of processing steps to go from ore to component, as well as material wastage from excessive machining. This paper describes a new solid-state hybrid manufacturing route, termed by the authors as FAST-*forge*, for converting titanium alloy powder into components with wrought properties in two steps; utilising field assisted sintering technology (FAST) to produce a shaped preform billet that is finished to near net shape by a one-step precision hot forge. The route has been demonstrated at the laboratory scale using Ti-6Al-4V hydride-dehydride powder by producing fully consolidated, microstructurally homogeneous, double truncated cone specimens directly through FAST, which were then upset forged at a range of temperatures and strain rates. The microstructural evolution and forging behaviour of the Ti-6Al-4V after FAST consolidation is similar to conventional melt, multi-step forged product. Break up of primary α at high strains was observed at 950°C and 0.01 s^{-1}, 0.1 s^{-1}, and 1 s^{-1}. There is good agreement between finite element modelling of the hot forging and the experimental data, which will enable more complex shaped geometries to be produced via the proposed FAST-*forge* route in future. Such a route could be used to consolidate powder from a lower-cost alternative extraction method to become a disruptive technology that will enable a step-change in the economics of titanium components.

Keywords: Spark Plasma Sintering (SPS); Pulsed Electric Current Sintering (PECS); Field Assisted Sintering Technology (FAST); Ti-6Al-4V; thermomechanical processing; hot forging.

1. Introduction

Titanium alloys exhibit excellent properties such as a higher specific strength than steels, exceptional corrosion resistance, high melting point and low thermal expansion. Yet titanium's high affinity for embrittling interstitials, such as oxygen, requires inert atmospheres during extraction and downstream processing. Such requirements are reflected in the high cost of titanium mill product and its limited use in non-aerospace sectors. This cost can be approximately broken down into two main areas, which is illustrated by the example of 25 mm thick plate in Fig. 1. The first area is ingot production, accounting for around half of the total cost, which encompasses the ore handling, Kroll process extraction, alloying and melting; most commonly via vacuum arc remelting (VAR), sometimes in combination with electron beam or plasma arc cold hearth remelting. The remaining cost is found in the second area of downstream processing, which in this example is the thermomechanical processing of the VAR ingot; normally multi-stage forging and re-heats to generate the component shape and required properties. As the complexity of the final component increases so does the proportion of the cost from downstream processing due to additional costly steps, such as secondary forging and machining. An approach that targets cost reductions in both areas is required for titanium to compete with commodity metals in non-aerospace sectors. Combining an alternative extraction method with subsequent cost-effective downstream processing offers the potential for significant price decreases.

The opportunity presented by a viable lower-cost alternative to the sixty-year-old Kroll process has led to the development of multiple different approaches around the globe; an overview and discussion of a variety of these can be found in (Fray, 2008), with a selection briefly discussed here. In the UK, electro-deoxidation is being developed (Mellor et al., 2015), including the production of novel titanium alloys directly from synthetic rutile feedstock (Benson et al., 2016). Several methods are being investigated in the USA: using hydrogen during the Kroll process' chlorination stage to produce TiH_2 powder, which can then be densified and simultaneously dehydrided by a variety of methods, is reportedly occurring at the pilot-plant scale (Duz et al., 2016); performing nearly continuous sodium reduction of $TICl_4$ (Armstrong et al., 1999); and

electrowinning from carbothermally reduced titanium oxide (Withers, 2015). In South Africa the use of continuous metallothermic reduction of $TiCl_4$ in molten salt is being trialled (Van Vuuren et al., 2011). In Australia the use of continuous magnesium reduction of $TiCl_4$ in a fluidised bed reactor process is being explored (Doblin et al., 2012). All these alternative extraction processes produce a powder or particulate titanium product. Importantly, as Fig. 1 illustrates, alternative powder extraction routes alone will be insufficient to achieve the cost reduction necessary for sectors such as the automotive industry. It is the subsequent consolidation of powder into mill product and near net shape components that will have the most dominant effect on cost reduction. Cost savings can be made in downstream processing by removing as many of the traditional multi-stage thermomechanical processing steps as possible.

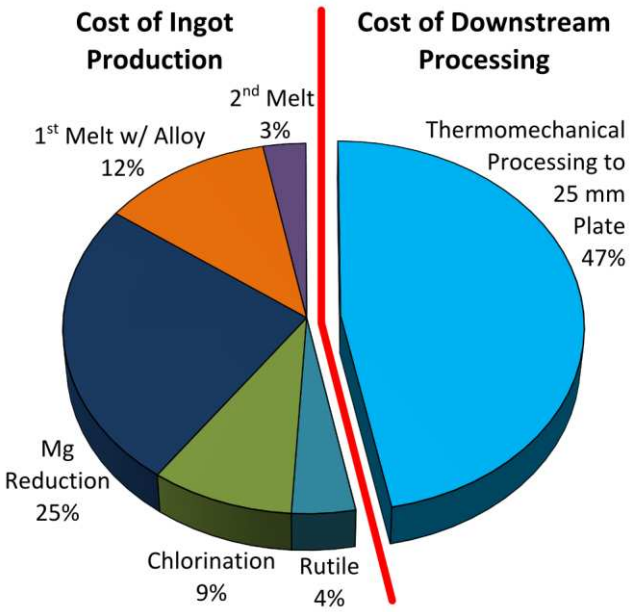

Fig. 1: Chart demonstrating the two main areas of production costs for 25 mm titanium alloy plate when conventionally processed; with relative cost factors for each sub-area also shown. Produced from data reported in (Kraft, 2004).

Traditional powder metallurgy techniques are able to densify powders without the need for melting, due to the mechanism of sintering; where adjacent surfaces bond due to diffusional processes that are enhanced by the application of heat (German, 2014). FAST, also known as spark plasma sintering, allows the solid-state consolidation of powders by combining the effects of high temperature with the application of uniaxial

pressure. The heat is generated through Joule heating as DC current is applied through a mould assembly containing the powder, either continuously or pulsed in a chosen pattern, which allows very high heating rates to be attained compared to more traditional sintering methods. Hydraulically actuated rams allow the application of axial mechanical load to produce the required pressure. FAST is considered an effective method for rapid sintering due to the high heating rates and the blend of heat and pressure; with broad agreement that it can produce equivalent or improved properties, compared with conventional techniques like hot isostatic pressing (HIP), whilst operating with reduced processing times and/or lower temperatures (Munir et al., 2011). This has allowed improved sintering of a range of materials, some that were customarily considered more problematic, such as WC (Orrù et al., 2009). The electric current appears to play a role in enhancing the sintering beyond simple Joule heating, and it is routinely proposed that high localised currents create the eponymous spark plasma, which increases sintering via a mechanism of particle surface cleaning or localised melting/evaporation. However, there is currently insufficient experimental evidence of spark plasma, suggesting that the term is misleading at best; Hulbert et al. were unable to detect it in a variety of powders across a wide spectrum of conditions using a range of techniques (Hulbert et al., 2008). In the absence of spark plasma, other authors have suggested the current might increase diffusion through improving mass transport by electromigration; increased neck growth of copper spheres with increasing current under FAST conditions of fixed temperature, pressure, and time has been shown (Frei et al., 2007). It is clear that complex mechanisms are operating to produce the enhanced sintering that is seen and they are not yet fully understood. From a cost saving perspective FAST may also offer benefits: a 90-95% energy saving has been claimed when using FAST to consolidate $TiAlO_2$ – TiC composites when compared to hot pressing, whilst also reporting a slight improvement in properties (Musa et al., 2009). There is an absence of published work on producing anything other than simple disc shaped specimens via FAST and therefore the limitations of this technology to produce complex geometries is currently unknown.

The authors previously indicated the capability of FAST in the sintering of a range of commercial and lower-cost titanium alloy powders (Weston et al., 2015). It was shown that FAST is tolerant of powder morphology and chemistry, and high heating rates could be used to lower processing times with minimal

95 effect on microstructure. Simple disc shapes of constant thickness achieved uniform powder packing and
96 consolidation with no density gradients, which allows microstructural homogeneity throughout specimens,
97 even when scaling up to larger sizes (250 mm diameter and 5 kg); additionally, it was shown that there was
98 limited pick-up (between 100-250 ppm) of carbon, oxygen, and nitrogen from the starting powders. The
99 ability to utilise feedstocks which are larger and angular, including potentially those from alternative
100 extraction methods or even recycled swarf, and still achieve high density and homogeneous microstructures
101 means that FAST has an advantage over traditional sintering operations as these feedstocks are lower-cost.
102 However, the authors believe that the geometries and mechanical properties required by most titanium
103 alloy components will not generally be producible by using FAST as a consolidation process in isolation. The
104 large-grained transformed β microstructure with grain boundary α is not optimal for components that need
105 a good balance of properties; a bi-modal microstructure, produced by hot-working in the α-β phase region,
106 offers advantages for most applications (Lütjering, 1998). The production of complex near net shape
107 geometries directly via FAST may be possible in the future with further investigation although the
108 microstructure would in all likelihood still need refining. Nonetheless, FAST of titanium powder has the
109 potential to be an effective intermediate consolidation and shaping process prior to further
110 thermomechanical processing in the form of a closed-die hot forging operation. To be the most efficient and
111 cost-effective it is possible, with sufficient process design and control, that this could be a one-step near net
112 shape forging operation. To achieve the desired final post-forge geometry and strain levels, and thus
113 microstructures, it is likely that the preform billet produced via FAST will need shape and definition. Finite
114 element (FE) modelling has become a common tool to provide load and microstructural predictions during
115 complex forging operations, although a comprehensive data set is required to achieve this. Therefore, from a
116 process modelling point of view the effect of thermomechanical processing parameters on microstructural
117 evolution needs to be understood due to their inevitable variation, even when nominally isothermal forging.
118 Levels of strain, strain rate and temperature can significantly affect the microstructure of titanium alloys and
119 a large test matrix would be needed to characterise this if using traditional cylindrical axisymmetric
120 compression specimens. The novel double truncated cone testing approach (Jackson et al., 2000) allows this

microstructural characterisation in far fewer tests due to the predictable and controlled strain distribution in the forged specimen. A double cone specimen can be tested at a set temperature and strain rate to give information relating to a larger range of strains, from almost zero at the edge to high strains in the centre. Small specimen dimensions can limit temperature variations so that a good approximation of isothermal forging can be realised, as well as allowing metallographic preparation and inspection of the entire specimen.

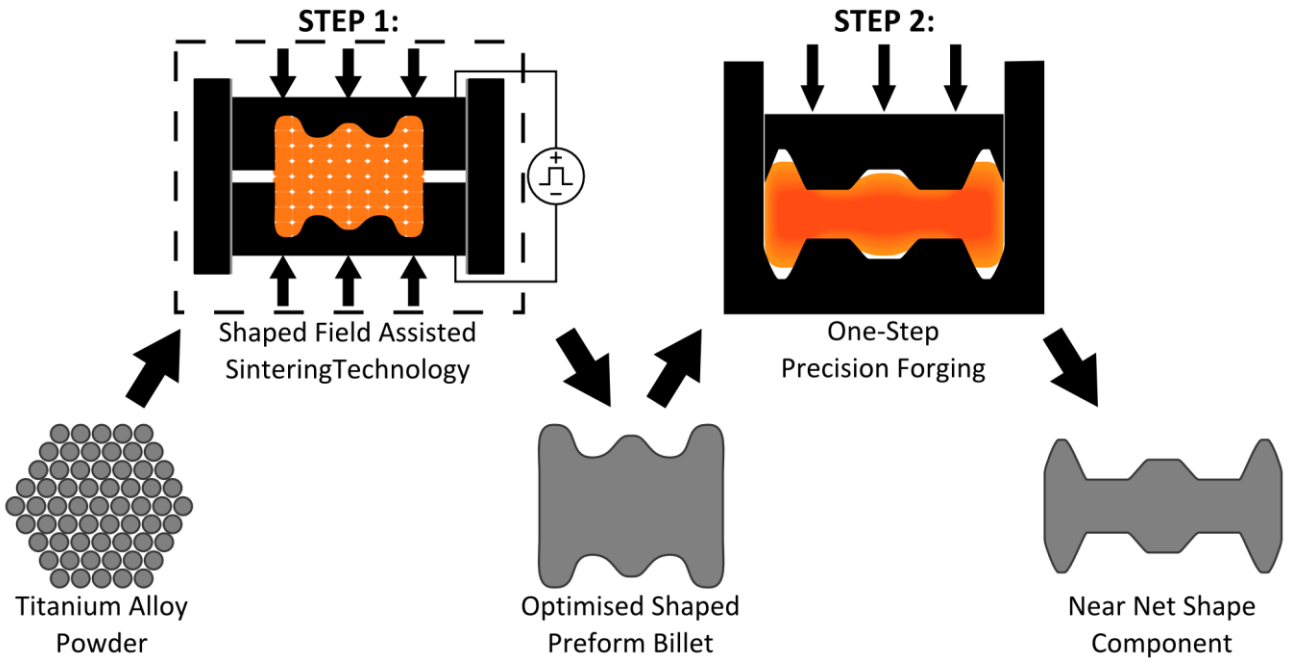

Fig. 2: Schematic diagram outlining the two-step hybrid "FAST-forge" process – a proposed cost-effective solid-state processing route for producing titanium alloy components from powder.

The aim of this paper is to demonstrate, at the laboratory scale, that it is possible to produce components from powder in two steps, as shown schematically in Fig. 2; using Field Assisted Sintering Technology (FAST) to produce a shaped preform billet, which is finished to near net shape with one-step precision forging. Depending upon the application it is envisaged that a subsequent heat treatment would allow tailoring of the microstructure if required and/or a minimal finish machining operation would produce an acceptable surface roughness. This novel solid-state hybrid processing route, termed by the authors as "FAST-*forge*", will allow manufacturing of components with forged properties for dynamically loaded applications from titanium alloy powders. It is hoped that the mechanical properties achieved by the additional forging of FAST

material will allow FAST-*forge* products to be used in areas and applications not conventionally considered possible for as-sintered PM components. It is envisaged that with further development FAST-*forge* will become disruptive technology for a range of sectors. The combination of this cost-effective consolidation method with powder from a lower-cost extraction method will provide a step-change in the economics of titanium components.

2. Materials and Methods

2.1 Experimental Approach

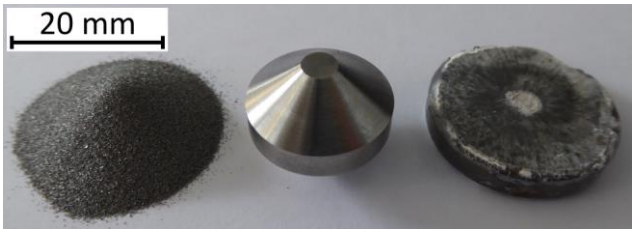

Fig. 3: Photograph demonstrating the outcome at each stage of the two-step FAST-forge process; the starting Ti-6Al-4V HDH powder (left) to the intermediate shaped preform billet, a double truncated cone FAST specimen with a light surface machine (centre), and the final forged specimen (right).

The experimental approach aimed to demonstrate three key developments. Firstly, the capability of FAST to produce shaped preforms to be used in the FAST-*forge* process. Secondly that the FAST-*forge* concept, of producing a component with wrought properties from powder in two steps, was viable through a laboratory-scale demonstration, see Fig. 3. Thirdly, to link microstructural evolution of FAST produced preforms to thermomechanical processing parameters by utilising the double truncated cone specimen geometry as the shaped preform billet; thus gaining valuable information for future process optimisation through FE modelling. Ti-6Al-4V hydride-dehydride (HDH) powder was used for this proof of concept demonstration, to enable comparison with conventional wrought product, as well as setting a benchmark for future work with lower-cost powder from an alternative extraction method.

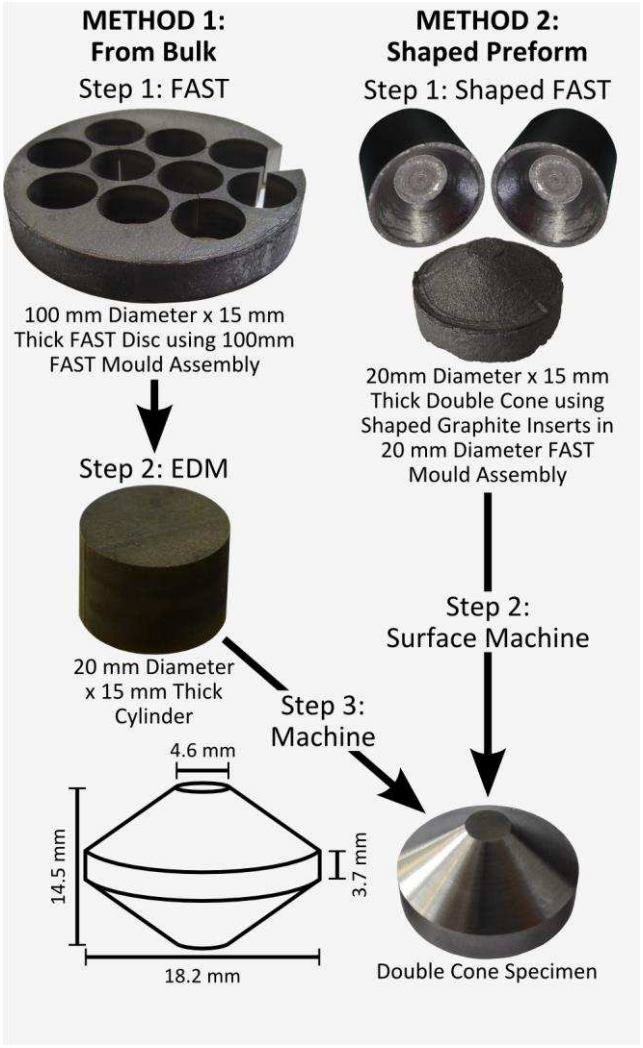

158

159 *Fig. 4: Schematic showing the two methods used to make the double truncated cone specimens. Method 1*
160 *produced a 100 mm diameter x 15 mm thick FAST disc, which smaller cylinders were extracted from via*
161 *electro-discharge machining (EDM), and then machined to the final dimensions shown (known as "bulk"*
162 *double cone specimens). Method 2 used shaped graphite inserts in a 20 mm diameter FAST mould assembly*
163 *to produce shaped preforms, which then had a surface machine to give the final dimensions shown (known as*
164 *"shaped" double cone specimens).*

165 Two methods were used to create the double cone specimens, see Fig. 4. The first method was to electrical
166 discharge machine 20 mm diameter x 15 mm thick cylinders from a 100 mm diameter x 15 mm thick FAST
167 disc, which were then machined to the final dimensions shown in Fig. 4 (known as "bulk" double cone
168 specimens hereafter). The second method was to produce shaped preforms by placing shaped graphite
169 inserts into a 20 mm diameter FAST mould assembly, which were also machined to the same final

dimensions (known as “shaped” double cone specimens hereafter). The same sintering cycle and hot compression testing conditions were applied for both methods of double cone specimen production. The aim of creating additional specimens from bulk material was to allow a comparison of behaviour with shaped preform specimens produced directly via FAST; thus demonstrating that the shaped FAST method does not adversely affect either the powder consolidation or subsequent forging response.

2.2 Materials

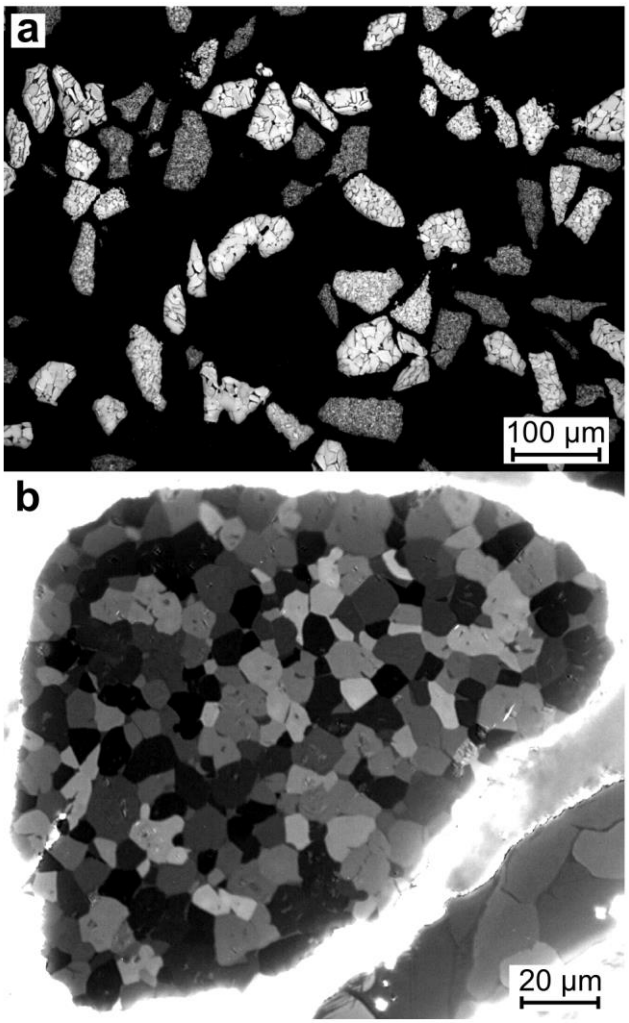

Fig. 5: Light micrographs of the Ti-6Al-4V HDH powder’s particle morphology after etching with Kroll’s reagent (a) and microstructure under cross-polarised light (b).

The Ti-6Al-4V HDH powder was purchased from Reading Alloys Inc., (an Ametek Company), Robesonia, PA, USA, and certified to contain 6.34% Al, 4.02% V, 0.21% Fe, 0.026% C, 0.016% H, 0.013% N, and 0.16% O;

181 therefore meeting the ASTM Grade 5 specification, except 0.001% excess hydrogen. The size range was
182 75-150 µm, with 96.7% of particles within these limits. The powder morphology was angular and irregular in
183 shape, see Fig. 5a, with a microstructure of equiaxed α grains approximately 5-10 µm in diameter, see Fig.
184 5b.

185 **2.3 Methods**

186 2.3.1 Field Assisted Sintering Technology

187 The FAST systems used to consolidate the powder in these experiments were manufactured by FCT Systeme
188 GmbH. The 100 mm disc used for the bulk double cone specimens was made using the Type H-HP D 250
189 system based at Kennametal Manufacturing (UK) Ltd. The shaped double cone specimens were made using
190 The University of Sheffield's Type HP D 25 system, see Fig. 6. The methodology was the same for both
191 machines. The mass of powder required (520 g for bulk and 15 g for shaped) was placed into a graphite ring
192 mould, simply between two graphite pistons for the bulk disc specimen, or with extra shaped graphite
193 inserts for the shaped double cone specimens. Graphite foil was used to line the mould assembly to aid with
194 specimen removal and prolong mould life. The mould assembly was then placed between the two
195 conducting hydraulic rams in the machine's vacuum chamber and held with a put-on load of 5 kN to ensure
196 good electrical contact was made. The sintering cycle used was as follows: the vacuum chamber was
197 evacuated, pulsed DC current was applied in the pattern of 15 ms on and 5 ms off. The values of current and
198 power rose steadily from initial values of 0.45 kA and 2.0 kW to 1.12 - 1.18 kA and 5.9 - 6.3 kW during the
199 dwell period for the shaped double cone specimens. The value of power for the 100 mm disc was a
200 maximum of 163 kW during the heating period and 37 - 42 kW during the dwell period (a sensor fault
201 prevented recording of current data). The heating was uncontrolled up to 450°C due to the operating limits
202 of the pyrometer. Above 450°C a constant heating rate of 100°Cmin^{-1} was used up to the dwell temperature
203 of 1200°C, points A-C in Fig. 6. Once 600°C was reached, point B, the pressure began to increase, with a rate
204 so that the maximum of 50 MPa would occur simultaneously with the maximum temperature, point C. A
205 dwell time of 30 minutes at maximum conditions was then used, points C-D. For the 100 mm bulk disc the

current was then turned off and the specimen allowed to “free” cool, points D-E. For the shaped double cone specimens, the current was used to achieve a “controlled” cooling rate to match the bulk disc cycle. The “controlled” cool is achieved by the FAST furnace software reducing the applied current to a level where the heat loss exceeds the Joule heat generated by the correct amount to attain the desired cooling rate. The pressure was also gradually decreased back to 5 kN during the cool.

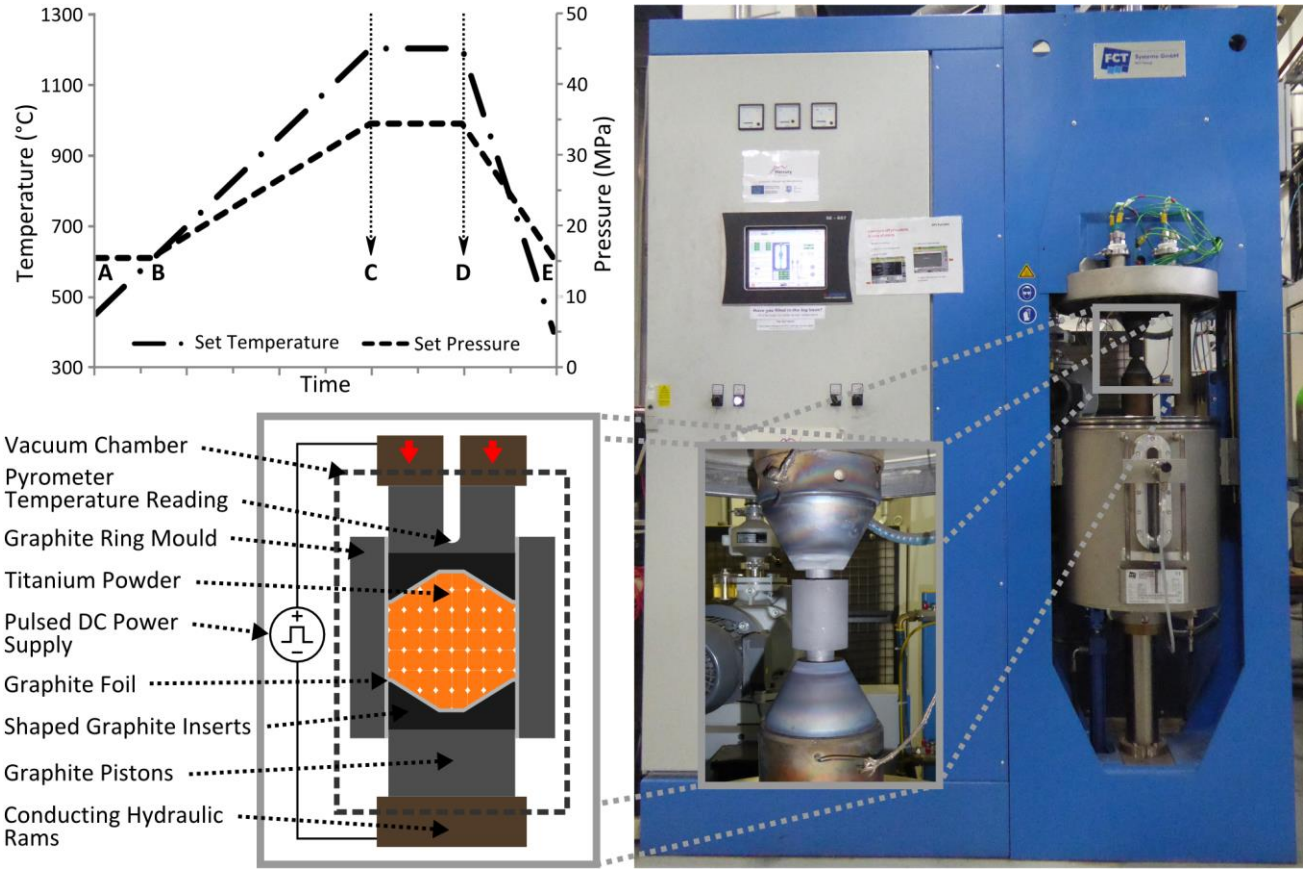

Fig. 6: Photograph of the FCT Systeme GmbH Type HP D 25 FAST Furnace at The University of Sheffield (right); showing detail of the graphite mould assembly held between the conducting hydraulic rams (inset right). Schematic cross-section showing the main components of the FAST system and mould assembly used (bottom left) and a graph outlining the variation in major processing parameters during a typical FAST cycle (top left).

2.3.2 One-Step Forging

The replication of the one-step forging stage was undertaken using The University of Sheffield’s thermomechanical compression testing machine, see Fig. 7. The test furnace contained two M22 steel tool

posts, where the upper one was servo-hydraulically actuated, allowing a constant strain rate deformation to a strain of 1.15. A fast thermal treatment unit (FTTU), located immediately in front of the test furnace, allowed induction heating of the double cone specimens at 4°Cs^{-1} to the test temperature, with a hold of 30 seconds to minimise any oscillation.

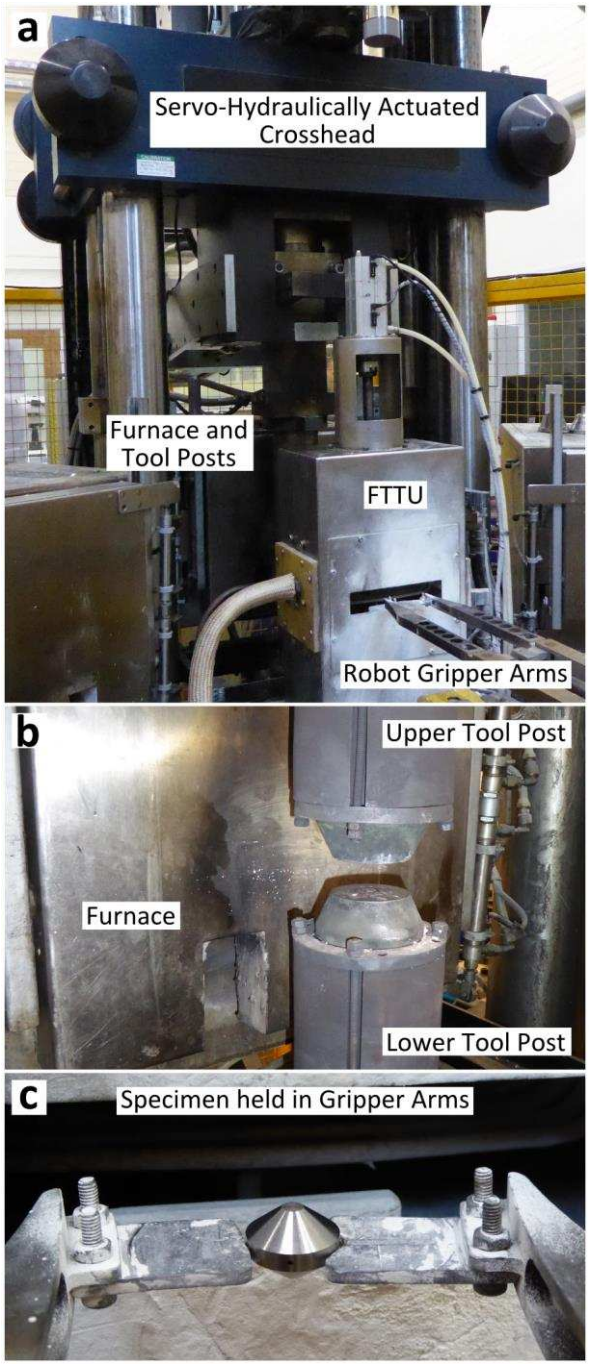

Fig. 7: Photographs outlining the major components of The University of Sheffield's thermomechanical compression machine (a), close-up view of the tool posts and furnace (b) (note the furnace has been moved

to the rear to enable viewing of the tool posts), close-up of a double truncated cone specimen held in the robot gripper arms (c).

Robot gripper arms were used to manipulate the specimen during testing; allowing positioning at the correct height before automatically moving into the FTTU and then into the test furnace for the one-step forge, followed by specimen withdrawal for a water quench. A 1.1 mm hole located centrally in the edge of the double cone specimens allowed an N-type thermocouple to be attached; giving control during induction heating and temperature data during deformation. A boron nitride coating was applied to limit interstitial pick up and reduce friction. A data logger recorded time, temperature, load, velocity, and displacement information throughout the test. Bulk double cone specimens were deformed at 850°C, 950°C, and 1050°C, and at strain rates of 0.01 s^{-1}, 0.1 s^{-1} and 1 s^{-1}. The shaped double cone specimens were deformed at 950°C, at strain rates of 0.01 s^{-1}, 0.1 s^{-1} and 1 s^{-1}.

2.3.3 Finite Element Simulation of the One-Step Forge

The finite element software DEFORM^{TM}(Scientific Forming Technologies Corporation, 2016) was used to simulate the compression tests of the double cone specimens to give the strain profiles across the specimens seen in Fig. 11a-11c. These strain profiles allow the linking of microstructural evolution to thermomechanical processing parameters (strain, strain rate, temperature). Due to the axisymmetric nature of the specimens it was possible to use a 2-D model of half the double cone geometry, meshed with 3160 elements, which simplified the simulation and reduced processing time. Rheology data from previous unpublished work, in a tabular form (stress values at a range of strains for each testing condition), was used for the material model, see Table 1 in the appendix. The material response was assumed to be fully plastic. For each test condition the initial temperature was set to that recorded by the thermocouple at the start of the experimental compression, and the measured temperature profile during the tests was used as a boundary condition for the specimen ensuring the simulation matched the experimental conditions as closely as possible. Two non-meshed rigid platens were used to represent the tool posts as their experimental deformation can be treated as negligible. The movement of the upper platen was controlled by setting a condition to produce a

constant global average strain rate to match the experiment; the software determined the magnitude of displacement necessary to achieve the set strain rate for each time step. Contact boundary conditions between the specimen and platens were established with a constant shear friction factor ($\bar{m}$) of 0.3.

2.3.4 Metallography

Typical metallographic preparation for Ti-6Al-4V was used for all specimens: sectioned in half parallel to the compression direction, hot-mounted in Bakelite, followed by grinding using progressively finer SiC papers then 9 µm diamond suspension, and finally chemical/mechanical polishing using colloidal silica of 0.05 µm with 20% hydrogen peroxide. Microstructural observations were performed using a Nikon Eclipse LV150 light microscope under reflected light conditions, either in bright field or polarised light mode. Kroll's reagent was applied as an etchant, if needed, until increased microstructural detail was visible.

3. Results and Discussions

3.1 Microstructures after FAST

Preliminary experiments demonstrated that the initial cooling rate after the current is turned off was significantly higher for the 20 mm diameter mould assembly at ~20 °Cs^{-1} than for the 100 mm diameter mould at ~0.33 °Cs^{-1}, see Fig. 8a. There is greater thermal mass for the larger mould assembly due to the increased amount of graphite required and it therefore takes longer to cool. This work sought to emulate the bulk material as closely as possible to allow direct comparison and therefore a "controlled" cool to match the "free" cool of the bulk was utilised for the shaped double cone specimen. The difference in microstructure produced by free and controlled cool can be seen in Fig. 8b and 8c; as expected the quicker free cool produced much finer α laths, where the controlled slower cool coarsened them to a size similar to the bulk specimen (directly compared in Fig. 9.)

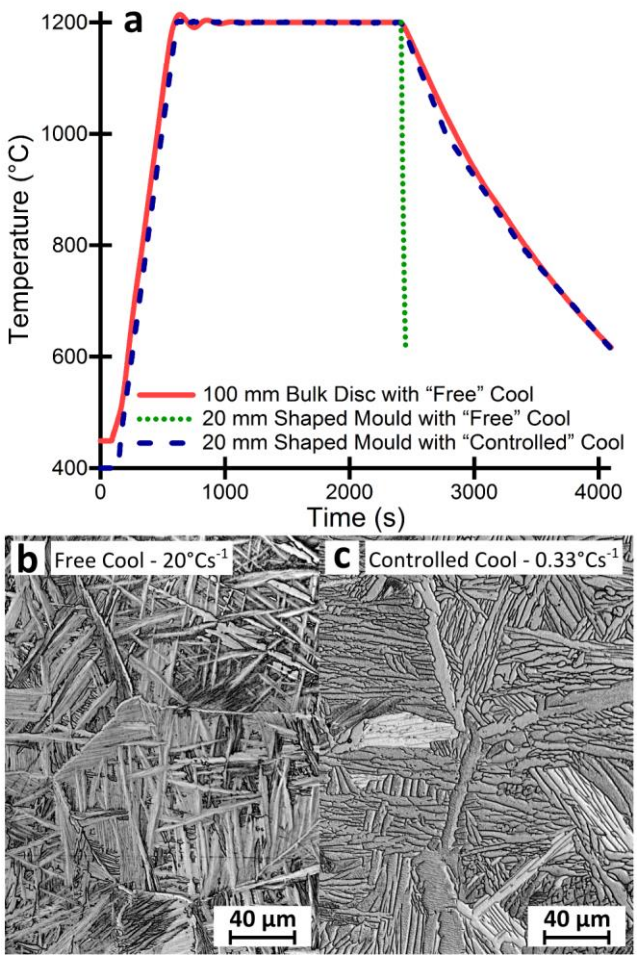

Fig. 8: Graph showing the temperature profiles during FAST processing of three types of Ti-6Al-4V specimen (a). A 100 mm diameter disc used for bulk double cone specimens; allowed to "free" cool after current switch-off (solid line). A 20 mm shaped mould when allowed to "free" cool after current switch-off (dotted line) with associated microstructure (b). A 20 mm shaped mould with "controlled" cool (dashed line) and associated microstructure (c).

The microstructures produced in this work when consolidating the Ti-6Al-4V HDH powder using FAST at a heating rate of 100°Cmin^{-1} with dwell conditions of 1200°C and 50 MPa held for 30 minutes are shown in Fig. 9. A typical microstructure of the 100 mm diameter disc used to produce the bulk double cone specimens is shown, as are micrographs from selected locations throughout the shaped double cone specimens. Both specimen types show the expected transformed β microstructure that is characteristically found when slow cooling from above the β transus temperature; prior β grains containing α laths in a Widmanstätten or

284 colony structure with some amount of α phase present on the grain boundaries (Joshi, 2006). The prior β
285 grain size ranges from approximately 200-600 μm with an α lath width in the region of 3-10 μm. The high
286 temperature and level of consolidation during the dwell period allowed β grain growth beyond the
287 dimensions of the initial powder particles for both bulk and shaped specimens, which is a significant change
288 in microstructure from the starting powder. This β grain growth demonstrates the high density achieved as
289 at lower levels of consolidation the remaining porosity acts to pin grain boundaries and prevent growth.
290 Image analysis, using the software ImageJ (Rasband, 1997), of multiple bright-field micrographs across each
291 specimen allowed the calculation of density as 99.88% for the shaped double cone specimens and as 99.87%
292 for the bulk double cone specimens. These values are slightly greater than the 99.01% stated by (Xu et al.,
293 2014) and slightly less than the 99.9% reported by (Kim et al., 2014) for HIP of Ti-6Al-4V powders, which
294 claimed to have tensile strength and elongation comparable to wrought material. The porosity will also be
295 healed further during the forging process, which will further increase tensile properties and more
296 importantly fatigue strength.

297 It can also be seen in Fig. 9 that microstructural homogeneity was achieved in the shaped double cone
298 specimen, with comparable micrographs from top to bottom and from centre to edge. Graphite has a higher
299 electrical resistivity than Ti-6Al-4V and consequently acts as the main heating element in the mould
300 assembly. Thus, it was hypothesised that a shaped mould, with non-uniform graphite thickness in the axial
301 direction, would produce uneven heating as well as a more complex pressure distribution that would lead to
302 microstructural variations; although this is not observed in the shaped double cones at this scale. If
303 temperature variations were present, they were small enough not to have had a significant effect at the
304 processing conditions used for these experiments. Although this may not be the case if a lower processing
305 temperature is required, especially as the β transus temperature is approached, where there will be a
306 reduction in the diffusional rates with increasing α content. It should be noted that the shape used here is
307 still a relatively simple axisymmetric profile and that further experimentation will be needed, with the aid of
308 FE modelling, to fully understand the difficulties involved in producing semi-complex shaped preform billets
309 as part of the FAST-*forge* processing route.

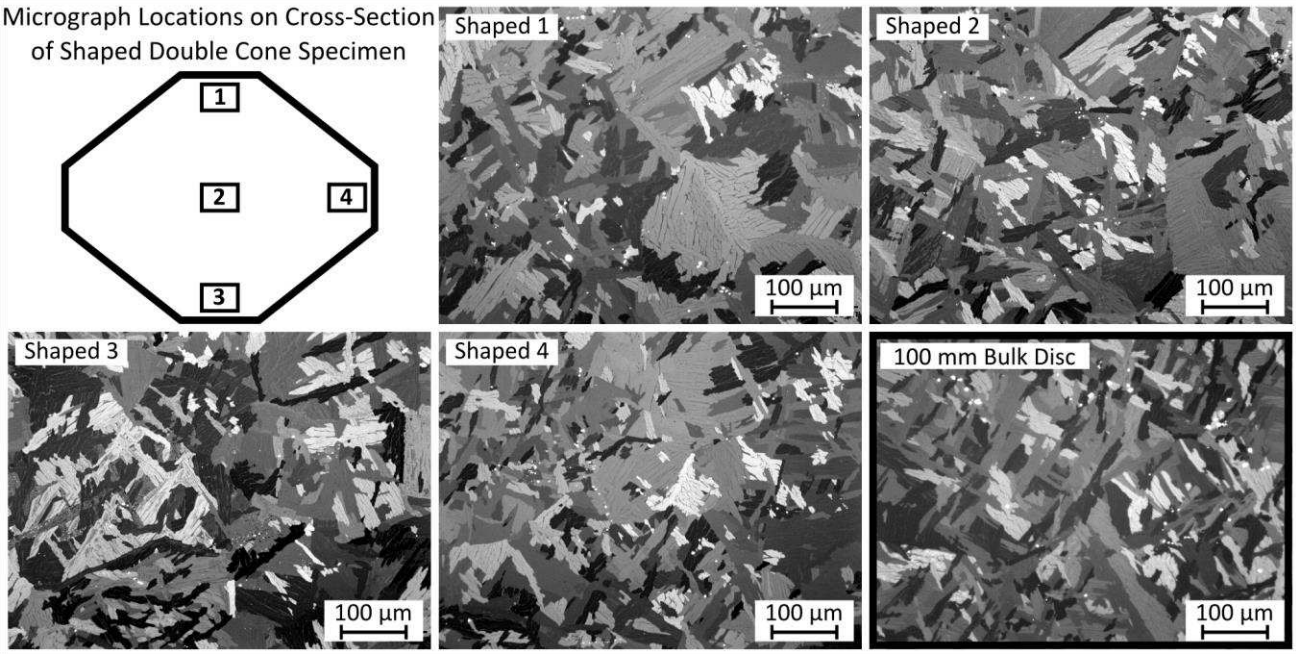

Fig. 9: Micrographs of Ti-6Al-4V double truncated cone specimens produced via FAST at a dwell temperature of 1200°C. Showing microstructures from a shaped specimen (Shaped 1-4) at the locations outlined in the top left diagram; and a characteristic microstructure of the homogeneous bulk specimen (bottom right).

3.2 Experimental Load-Displacement Curves

Due to the non-uniform cross-sectional area of the double cone specimens it is not possible to produce meaningful plots of stress versus strain during the thermomechanical compression. Consequently, the data is presented as plots of load versus displacement, which can be seen in Fig. 10 for deformations at 950°C and a range of strain rates. The effect of strain rate is clearly demonstrated; as the rate of deformation increases so does the force required to achieve equivalent displacement. The influence of temperature can be seen in the load-displacement curves at 850°C, 950°C, and 1050°C, see Fig. 12, where there is a marked reduction in the load required for equivalent displacement as temperature increases due to an increase in the more easily deformed β phase and an increase in dynamic recovery and recrystallisation processes. There are some small variations between the load-displacement behaviour of shaped double cone and bulk double cone specimens; at 1 s^{-1} the bulk specimen required a slightly higher load, at 0.1 s^{-1} the bulk specimen required a slightly lower load, and at 0.01 s^{-1} the bulk specimen required a higher load initially before finishing requiring a lower load. The level of variation seen is minimal and would be expected even when

testing duplicate samples from the same parent material due to attempting to control the large number of variables seen during hot working of metals. Frictional variations were limited by using similar quantities of lubricant for each test and cleaning the tool posts between tests, but small differences would still occur. The strain rate was closely controlled by the testing software and whilst small oscillations around the set value occurred these were the same for every test and it is thought not large enough to cause the variations in load seen. Due to less than perfect control of the heating in the FTTU causing small oscillations around the target test temperature, typically ±5°C, there was some variation in the initial temperature between samples, which would also have a small effect on the loads required.

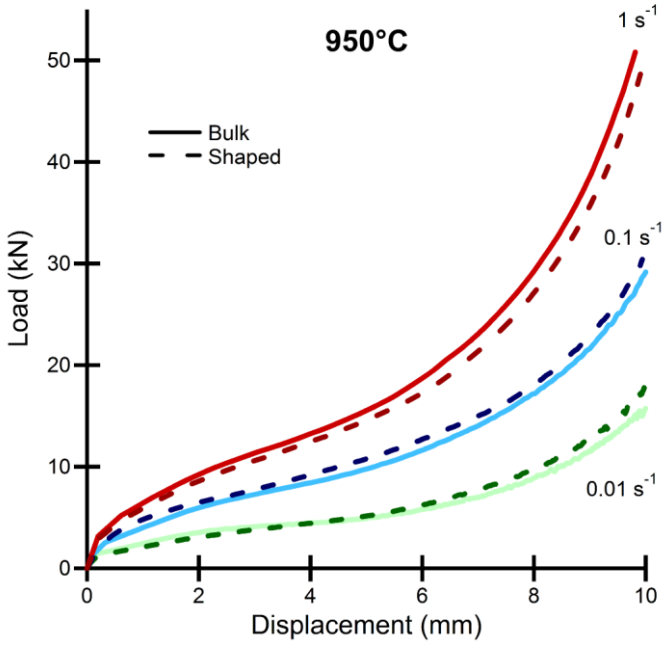

Fig. 10: Graphs of load-displacement curves during hot upset forging of Ti-6Al-4V double truncated cone specimens at 950°C and strain rates of 0.01 s^{-1}, 0.1 s^{-1}, and 1 s^{-1}. Bulk (solid lines) and shaped (dashed lines).

3.3 Microstructure Evolution Post One-Step Forging

The microstructural evolution for both bulk and shaped double cone specimens under hot uniaxial compression at 950°C, for strain rate regimes of 0.01 s^{-1}, 0.1 s^{-1} and 1 s^{-1} is shown in Fig. 11a-11c respectively. The location of the light micrograph images, 3 mm apart along the specimen centreline, is also marked on the FE simulation generated strain profile.

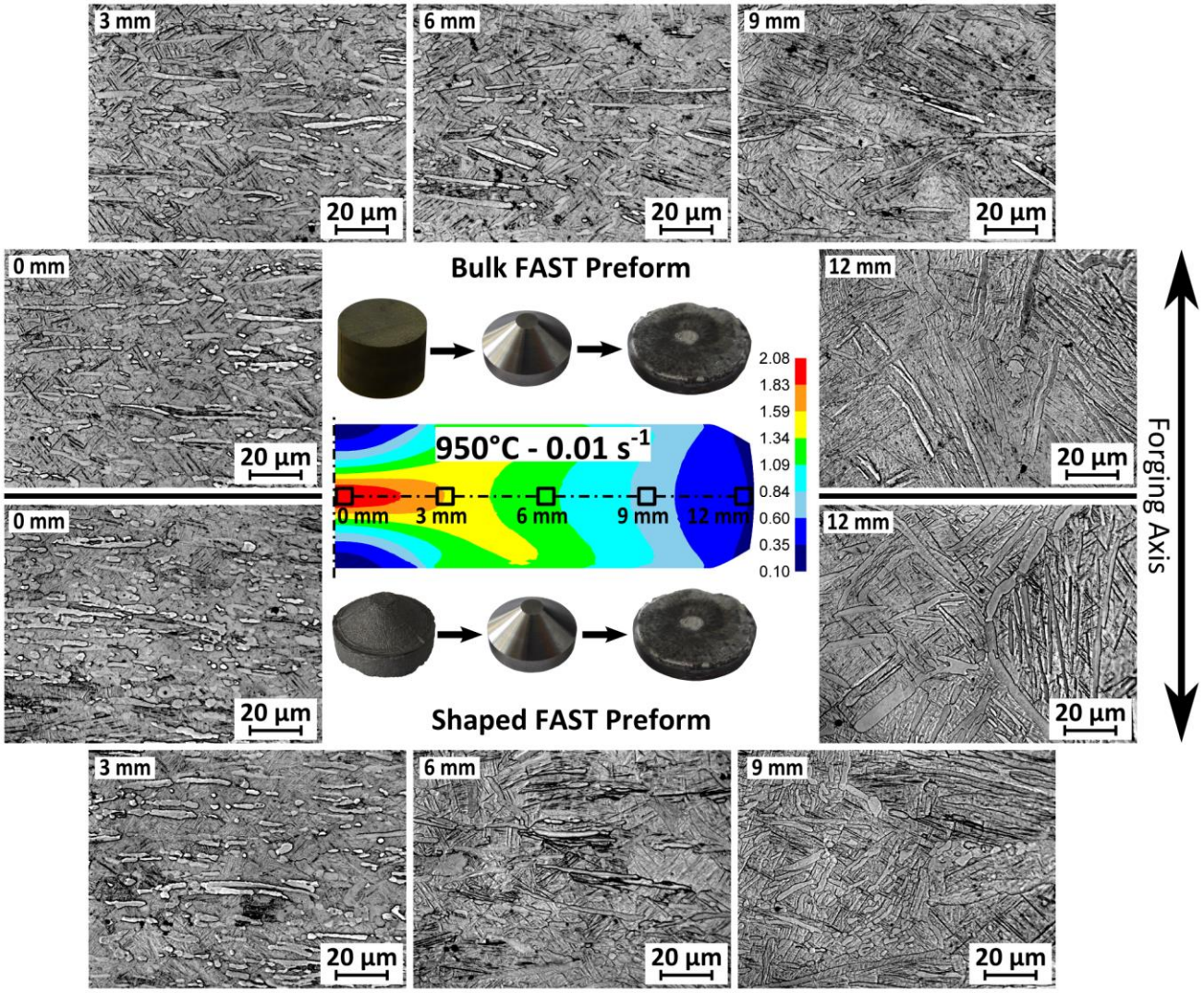

343

344 *Fig. 11a: Light micrographs of the microstructural evolution with increasing strain from edge to centre of the*

345 *double truncated cone specimens after forging at 950°C and 0.01 s^{-1}; produced from bulk (top) and via*

346 *shaped FAST (bottom).*

347 At low strains, 12 mm from the centre, there is slight coarsening of the primary α and the transformed β

348 grains manifest a finer secondary α lath structure than post-FAST due to the water quench and higher

349 cooling rate. As strain increases, moving towards the specimen centre, it can be seen across both bulk and

350 shaped double cone specimens at all strain rates that primary α platelets rotate and tend to align

351 perpendicular to the forging axis; all primary α appears to be fully aligned 6 mm from the centre (a strain of

352 ~1.1). At higher strains break-up of the α platelets into approximately 1-5 µm spheroidal α particles is

observed. As strain rate increases the time for diffusion dominated globurisation of primary α platelets decreases and it can be seen the amount of spheroidal α particles decreases from Fig. 11a-11c.

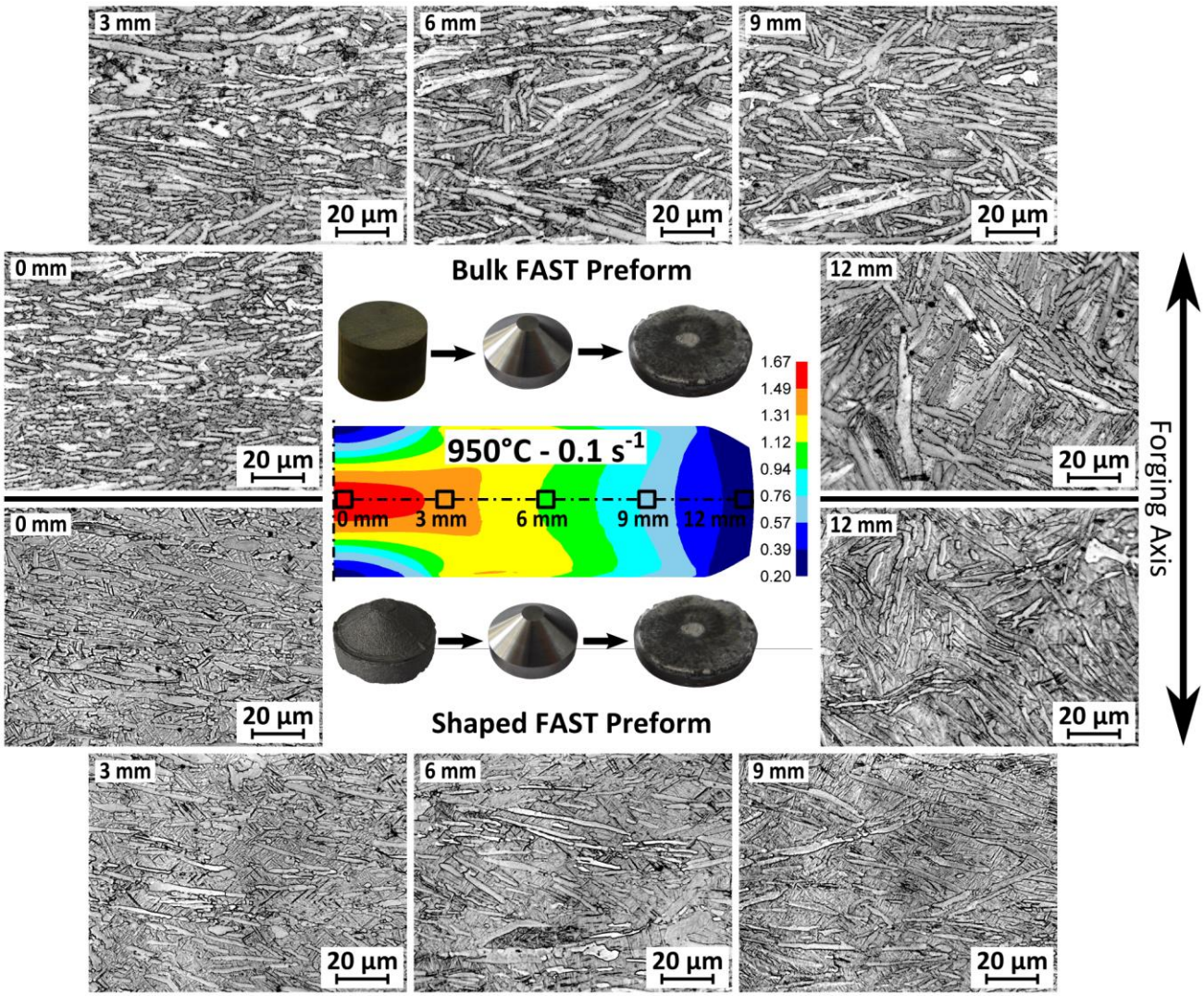

Fig. 11b: Light micrographs of the microstructural evolution with increasing strain from edge to centre of the double truncated cone specimens after forging at 950°C and 0.1 s^{-1}; produced from bulk (top) and via shaped FAST (bottom).

The microstructural evolution of shaped double cone specimens compared to double cone specimens machined from bulk is similar for all strain rates and strains. There has been a significant coarsening of the primary α in both the bulk double cone specimen at 0.1 s^{-1} and the shaped double cone specimen at 1 s^{-1}. This is due to these specimens failing to remain in the robot gripper arms upon retrieval from the test furnace so that the quenching did not occur automatically and a slower initial cool was experienced; the

specimens were manually quenched to room temperature approximately 60-120 s after forging. This slower cooling rate somewhat hinders a direct comparison between the two specimen types; however, the same microstructural trends are observed. The observed microstructural evolution is comparable to that reported during the hot working of conventionally produced Ti-6Al-4V with a colony α microstructure, as reported by (Semiatin et al., 1999).

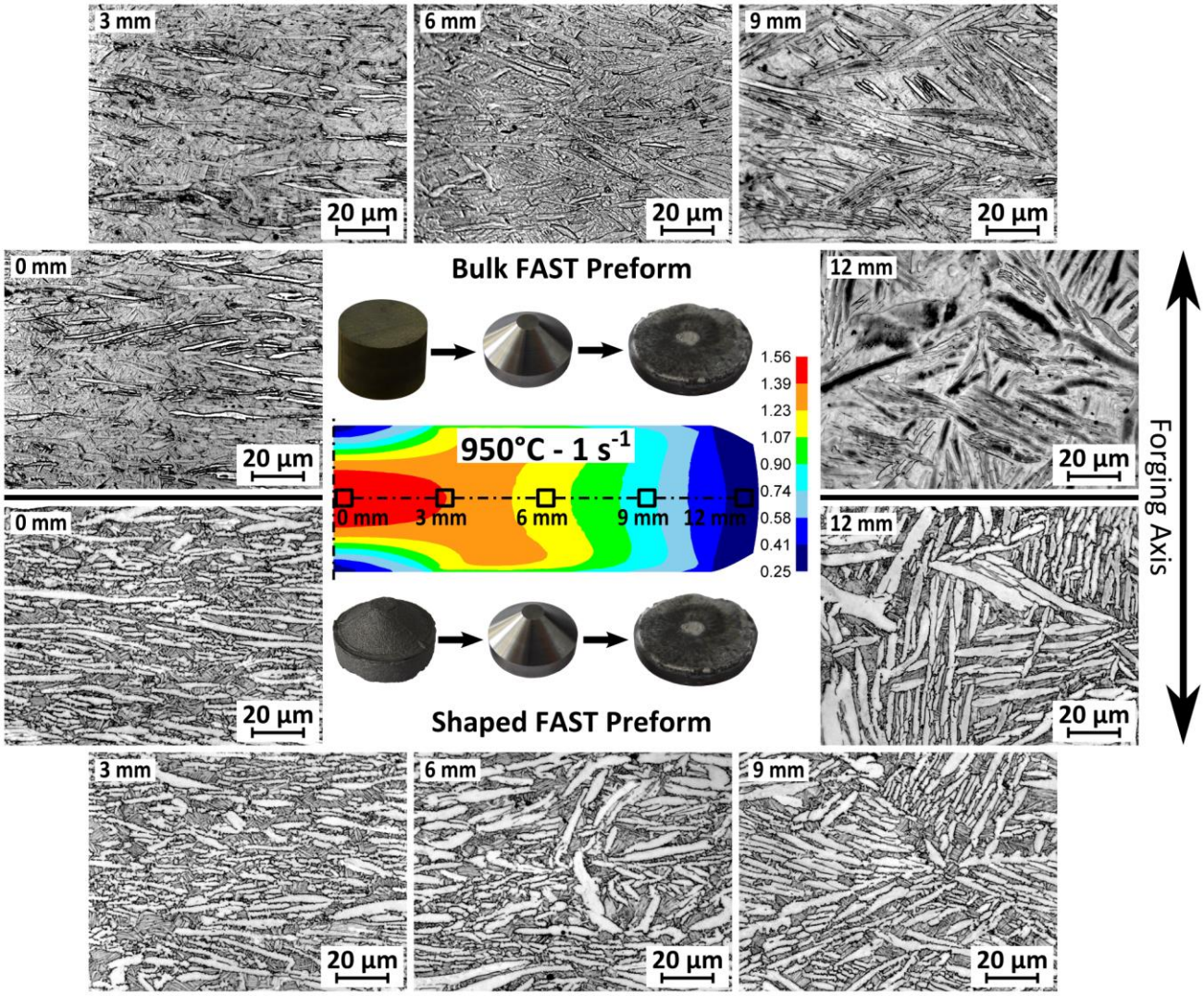

Fig. 11c: Light micrographs of the microstructural evolution with increasing strain from edge to centre of the double truncated cone specimens after forging at 950°C and 1 s^{-1}; produced from bulk (top) and via shaped FAST (bottom).

3.4 Finite Element Simulation

The load upon the upper tool with respect to its stroke (displacement) was extracted from the data produced by running FE simulations of each experimental point in the test matrix. This data is plotted against the experimentally recorded values of load and displacement for the bulk double cone specimens in Fig. 12. Only data for the bulk double cone specimens is shown to allow clearer comparison, as it has been shown that the shaped double cone specimens produced very similar load data. Overall there is good visual agreement between experimental and predicted values, which gives confidence that the predicted strain profiles are accurate. However, there is slight under prediction at 850°C and 950°C, but slight over prediction at 1050°C. The simulation was set up to mirror the recorded temperature profiles of the experiment, which due to adiabatic heating were not fully isothermal, therefore load changes due to temperature variability were accounted for. However, the material model used was discrete tabulated data (at temperatures of 850°C, 950°C, and 1050°C and strain rates of 0.01 s^{-1}, 0.1 s^{-1}, and 1 s^{-1}) with linear interpolation between conditions, which may not be realistic. A constant shear friction factor ($\bar{m}$) of 0.3 was used and appears to give good visual agreement with experimental conditions, using boron nitride as a release agent, as the end shape of the simulated curves largely matches the experimental even if the absolute values differ. Friction only has a large effect at higher displacements where the contact area has increased; it can be seen in the 850°C at 0.01 s^{-1} curve that a good match is achieved early in the test but the curves diverge at the end, which suggests that this test occurred under increased friction conditions. The material used to produce the data for the FE model was Ti-6Al-4V HDH powder processed in an 80 mm mould with a similar FAST cycle to this work, except a lower pressure of 21 MPa and allowed to free cool; the cooling rate was intermediate to those demonstrated in Fig. 8 and produced a transformed β microstructure with α laths of intermediate thickness to those shown here. This difference in starting microstructure may also explain some of the disparities between simulation and experiment. It should be noted that as tabulated data has been used the FE model can only be employed with confidence within the processing window defined by the extremes of the experimental conditions.

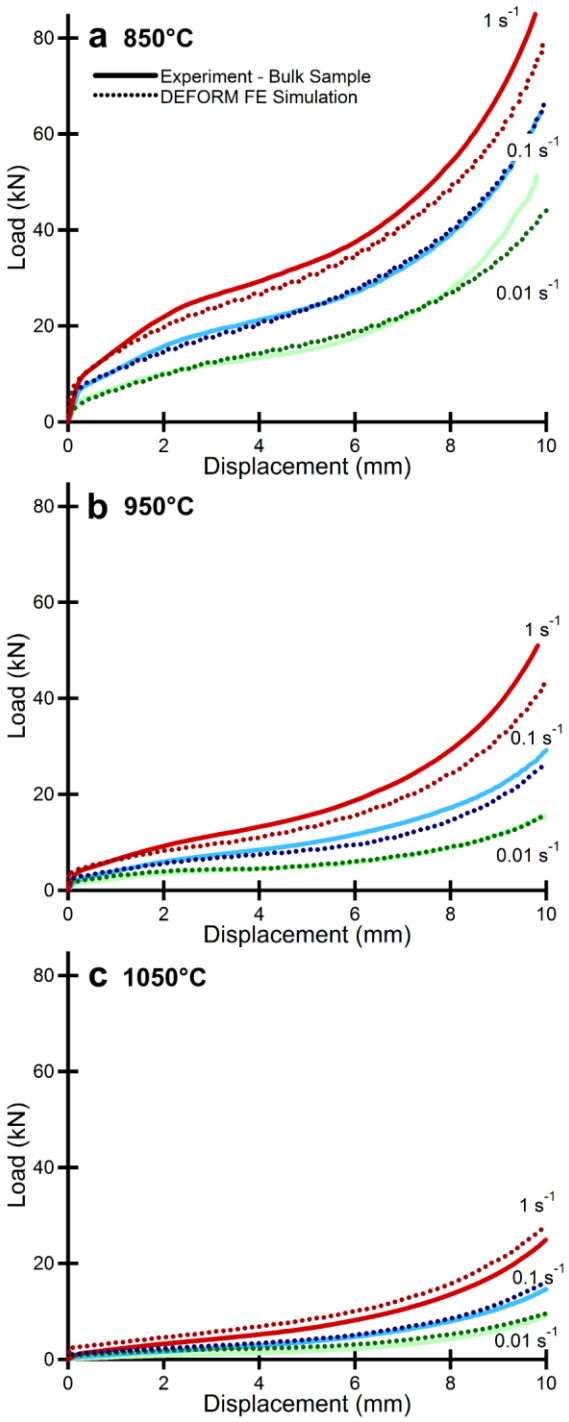

399

400 *Fig. 12: Graphs comparing the load-displacement curves during the upset forging of double truncated cone*

401 *specimens at 850°C (a), 950°C (b) and 1050°C (c) at strain rates of 0.01 s^{-1}, 0.1 s^{-1} and 1 s^{-1} (as labelled); from*

402 *bulk FAST material (solid lines) against those obtained from DEFORM™ FE simulation (dotted lines).*

403

404

4. Conclusions

- This paper has demonstrated at the laboratory scale that it is possible to produce a fully dense and microstructurally refined forged titanium alloy specimen in only two steps from powder. In the long-term the authors believe that this proposed cost-effective hybrid processing route, termed FAST-*forge*, combined with a lower-cost powder from an alternative extraction method will be disruptive technology that will enable a step-change in the economics of titanium alloys.
- Directly producing shaped FAST double cone specimens did not negatively affect microstructural or deformational behaviour when compared to double cone specimens machined from homogeneous bulk material. There is very good visual correlation between the two types of specimens. This establishes that using FAST to produce shaped preforms has the potential to be an effective intermediate step in the FAST-*forge* process. Further work is required to explore the possibilities and limitations of the technology prior to scale-up, but in future it should be possible to accurately produce shaped FAST preforms for a variety of final components.
- At the current level of FAST technology commercially available the cost-effectiveness achieved by the FAST-*forge* processing route will vary from component to component; an economic assessment on case by case basis would be required. The initial set-up costs may negate benefits for small batch production and speed of processing limitations may exclude products requiring continuous or very large/quick batch production. However, with expensive feedstocks such as titanium there may still be cost reductions to be found via FAST-*forge*. The tooling costs for FAST compare favourably against HIP, where the steel can bonds to the titanium and needs to be machined away, as the majority of the graphite mould assembly is reusable. The longevity and cost-effectiveness of the mould assembly in terms of both material and geometry needs to be investigated further to give an understanding of tooling costs as the technology progresses in size and part complexity.

- The response of Ti-6Al-4V FAST material under forging conditions is very similar to that seen when thermomechanically working conventional Ti-6Al-4V billet material; post-sintering FAST preforms have characteristics similar to conventional melt, multi-step forged product.
- The agreement between experimental load-displacement data and FE simulation data gives confidence that the material model utilised can be used to model the forging of more complex geometries as the FAST-*forge* process develops.
- Initial examination of the microstructural evolution indicates the level of strain, temperature and strain rate required to break up the post FAST microstructure and achieve a bimodal α-β microstructure, but further analysis is needed to tie key microstructural features to thermomechanical processing parameters for use in a simple microstructural prediction model.
- It is further anticipated that if the required mechanical properties of a component are identified then a microstructure necessary to meet these can be predicted. Using FE simulation, linked to a microstructural model, the shape of the preform could be iteratively optimised so that the one-step precision forging operation can produce the correct levels of strain at the forging conditions to yield the appropriate microstructure to meet the property requirements.

Acknowledgements

The authors acknowledge the Engineering and Physical Sciences Research Council's Advanced Metallic Systems Centre for Doctoral Training for funding N. S. Weston (Grant Number EP/G036950/1). Thanks go to the Defence Science and Technology Laboratory for additional funding, and specifically Dr Matthew Lunt for his support. The authors also recognise Dr Fatos Derguti for technical discussions and Dr Adam Tudball of Kennametal Manufacturing (UK) Ltd. for technical knowledge and assistance when using their large-scale FAST furnace.

Appendix

TABLE 1: Tabulated flow stress data at the indicated testing conditions and strain levels that was used as the material model for FE modelling of the forging of Ti-6Al-4V HDH powder consolidated using FAST at a heating rate of 100°Cmin^{-1} with dwell conditions of 1200°C and 50 MPa held for 30 minutes.

Strain	Test Conditions								
	850°C			950°C			1050°C		
	0.01 s^{-1}	0.1 s^{-1}	1 s^{-1}	0.01 s^{-1}	0.1 s^{-1}	1 s^{-1}	0.01 s^{-1}	0.1 s^{-1}	1 s^{-1}
0.000	0.0	0.0	0.0	0.0	0.0	0.0	0.0	0.0	0.0
0.010	31.3	98.4	94.0	24.7	50.3	39.6	7.2	20.0	43.3
0.015	57.7	146.3	149.1	30.6	58.0	57.6	8.8	28.1	44.0
0.020	90.5	175.6	188.2	32.1	60.5	72.4	10.0	31.5	45.0
0.030	111.5	192.0	213.4	34.0	60.2	75.5	10.6	32.6	46.3
0.050	114.9	192.3	220.4	34.3	59.3	78.5	11.5	33.4	47.4
0.100	114.5	188.0	225.4	34.8	58.4	82.9	12.4	34.1	48.6
0.150	112.5	183.7	227.5	34.6	57.4	87.3	13.2	34.4	49.7
0.200	110.0	178.1	229.6	33.6	56.3	89.5	14.1	34.1	50.8
0.250	106.9	172.8	231.5	33.0	54.8	89.8	14.9	33.7	51.9
0.300	105.1	168.1	228.1	32.4	53.8	89.9	15.8	33.2	53.0
0.400	98.8	160.0	218.5	31.5	51.9	88.7	16.3	32.2	53.3
0.500	95.6	153.7	208.5	30.6	50.7	87.6	16.8	31.2	53.0
0.600	92.6	147.8	202.1	30.1	50.5	87.2	16.2	30.8	53.1
0.700	89.1	143.4	195.4	29.7	50.2	87.2	15.3	30.3	53.1
0.800	84.1	138.4	189.8	29.3	50.2	87.2	14.9	30.2	53.1
0.900	82.1	135.6	187.8	29.0	50.2	87.2	14.2	30.2	53.1
1.000	79.3	135.2	186.6	28.6	50.2	87.2	13.8	30.2	53.1
1.200	73.8	135.2	186.6	28.2	50.2	87.2	12.8	30.2	53.1
5.000	73.8	135.2	186.6	28.2	50.2	87.2	11.5	30.2	53.1

References

Armstrong, D.R., Borys, S.S., Anderson, R.P., 1999. Method of making metals and other elements from the halid vapor of the metal. US5958106 A.

Benson, L.L., Mellor, I., Jackson, M., 2016. Direct reduction of synthetic rutile using the FFC process to produce low-cost novel titanium alloys. J. Mater. Sci. 51, 1–12. doi:10.1007/s10853-015-9718-1

Doblin, C., Chryss, A., Monch, A., 2012. Titanium powder from the TiRO^{TM} process. Key Eng. Mater. 520, 95–100. doi:10.4028/www.scientific.net/KEM.520.95

Duz, V.A., Matviychuk, M., Klevtsov, A., Moxson, V., 2016. Industrial application of titanium hydride powder. Met. Powder Rep. doi:10.1016/j.mprp.2016.02.051

Fray, D.J., 2008. Novel methods for the production of titanium. Int. Mater. Rev. 53, 317–325. doi:10.1179/174328008X324594

Frei, J.M., Anselmi-Tamburini, U., Munir, Z.A., 2007. Current effects on neck growth in the sintering of copper spheres to copper plates by the pulsed electric current method. J. Appl. Phys. 101, 114914-1-114914–8. doi:10.1063/1.2743885

German, R.M., 2014. Sintering: From Empirical Observations to Scientific Principles, Elsevier Inc. doi:10.1016/B978-0-12-401682-8.00011-2

Hulbert, D.M., Anders, A., Dudina, D. V., Andersson, J., Jiang, D., Unuvar, C., Anselmi-Tamburini, U., Lavernia, E.J., Mukherjee, A.K., 2008. The absence of plasma in “spark plasma sintering.” J. Appl. Phys. 104, 33305. doi:10.1063/1.2963701

Jackson, M., Dashwood, R.J., Christodoulou, L., Flower, H.M., 2000. Application of novel technique to

examine thermomechanical processing of near β alloy Ti–10V–2Fe–3Al. Mater. Sci. Technol. 16, 1437–1444. doi:10.1179/026708300101507433
Joshi, V.A., 2006. Titanium Alloys: An Atlas of Structures and Fracture Features, 1st ed. CRC Press Taylor & Francis Group, LLC.
Kim, Y., Kim, E.-P., Song, Y.-B., Lee, S.H., Kwon, Y.-S., 2014. Microstructure and mechanical properties of hot isostatically pressed Ti–6Al–4V alloy. J. Alloys Compd. 603, 207–212. doi:10.1016/j.jallcom.2014.03.022
Kraft, E.H., 2004. Summary of emerging titanium cost reduction technologies, A Study Performed For US Department of Energy And Oak Ridge National Laboratory Subcontract 4000023694. Vancouver WA.
Lütjering, G., 1998. Influence of processing on microstructure and mechanical properties of (α+β) titanium alloys. Mater. Sci. Eng. A 243, 32–45. doi:10.1016/S0921-5093(97)00778-8
Mellor, I., Grainger, L., Rao, K., Deane, J., Conti, M., Doughty, G., Vaughan, D., 2015. Titanium Powder Production via the Metalysis Process, in: Qian, M., Froes, F.H. (Eds.), Titanium Powder Metallurgy: Science, Technology and Applications. Butterworth-Heinemann Ltd, Oxford, UK, pp. 51–67. doi:10.1016/B978-0-12-800054-0.00004-6
Munir, Z.A., Quach, D. V., Ohyanagi, M., 2011. Electric current activation of sintering: A review of the pulsed electric current sintering process. J. Am. Ceram. Soc. 94, 1–19. doi:10.1111/j.1551-2916.2010.04210.x
Musa, C., Licheri, R., Locci, A.M., Orrù, R., Cao, G., Rodriguez, M.A., Jaworska, L., 2009. Energy efficiency during conventional and novel sintering processes: the case of Ti–Al2O3–TiC composites. J. Clean. Prod. 17, 877–882. doi:10.1016/j.jclepro.2009.01.012
Orrù, R., Licheri, R., Locci, A.M., Cincotti, A., Cao, G., 2009. Consolidation/synthesis of materials by electric current activated/assisted sintering. Mater. Sci. Eng. R 63, 127–287. doi:10.1016/j.mser.2008.09.003
Rasband, W.S., 1997. ImageJ, ImageJ. U.S National Institutes of Health, Bethesda, Maryland, USA, http://imagej.nih.gov/ij/.
Scientific Forming Technologies Corporation, 2016. DEFORM™ (v.11.0.1), DEFORM 11.0.1. SFTC, Columbus, Ohio.
Semiatin, S.., Seetharaman, V., Weiss, I., 1999. Flow behavior and globularization kinetics during hot working of Ti–6Al–4V with a colony alpha microstructure. Mater. Sci. Eng. A 263, 257–271. doi:10.1016/S0921-5093(98)01156-3
Van Vuuren, D.S., Oosthuizen, S.J., Heydenrych, M.D., 2011. Titanium production via metallothermic reduction of TiCl4 in molten salt: Problems and products. J. South. African Inst. Min. Metall. 111, 141–148.
Weston, N.S., Derguti, F., Tudball, A., Jackson, M., 2015. Spark plasma sintering of commercial and development titanium alloy powders. J. Mater. Sci. 50, 4860–4878. doi:10.1007/s10853-015-9029-6
Withers, J.C., 2015. Production of Titanium Powder by an Electrolytic Method and Compaction of the Powder, in: Qian, M., Froes, F.H. (Eds.), Titanium Powder Metallurgy: Science, Technology and Applications. Butterworth-Heinemann Ltd, Oxford, UK, pp. 33–50. doi:10.1016/B978-0-12-800054-0.00003-4
Xu, L., Guo, R., Bai, C., Lei, J., Yang, R., 2014. Effect of Hot Isostatic Pressing Conditions and Cooling Rate on Microstructure and Properties of Ti-6Al-4V Alloy from Atomized Powder. J. Mater. Sci. Technol. 30, 1289–1295. doi:10.1016/j.jmst.2014.04.011

TABLE 1: Tabulated flow stress data at the indicated testing conditions and strain levels that was used as the material model for FE modelling of the forging of Ti-6Al-4V HDH powder consolidated using FAST at a heating rate of 100°Cmin^{-1} with dwell conditions of 1200°C and 50 MPa held for 30 minutes.

Fig. 1: Chart demonstrating the two main areas of production costs for 25 mm titanium alloy plate when conventionally processed; with relative cost factors for each sub-area also shown. Produced from data reported in (Kraft, 2004).

Fig. 2: Schematic diagram outlining the two-step hybrid "FAST-forge" process – a proposed cost-effective solid-state processing route for producing titanium alloy components from powder.

Fig. 3: Photograph demonstrating the outcome at each stage of the two-step FAST-forge process; the starting Ti-6Al-4V HDH powder (left) to the intermediate shaped preform billet, a double truncated cone FAST specimen with a light surface machine (centre), and the final forged specimen (right).

Fig. 4: Schematic showing the two methods used to make the double truncated cone specimens. Method 1 produced a 100 mm diameter x 15 mm thick FAST disc, which smaller cylinders were extracted from via electro-discharge machining (EDM), and then machined to the final dimensions shown (known as "bulk" double cone specimens). Method 2 used shaped graphite inserts in a 20 mm diameter FAST mould assembly to produce shaped preforms, which then had a surface machine to give the final dimensions shown (known as "shaped" double cone specimens).

Fig. 5: Light micrographs of the Ti-6Al-4V HDH powder's particle morphology after etching with Kroll's reagent (a) and microstructure under cross-polarised light (b).

Fig. 6: Photograph of the FCT Systeme GmbH Type HP D 25 FAST Furnace at The University of Sheffield (right); showing detail of the graphite mould assembly held between the conducting hydraulic rams (inset right). Schematic cross-section showing the main components of the FAST system and mould assembly used (bottom left) and a graph outlining the variation in major processing parameters during a typical FAST cycle (top left).

Fig. 7: Photographs outlining the major components of The University of Sheffield's thermomechanical compression machine (a), close-up view of the tool posts and furnace (b) (note the furnace has been moved to the rear to enable viewing of the tool posts), close-up of a double truncated cone specimen held in the robot gripper arms (c).

Fig. 8: Graph showing the temperature profiles during FAST processing of three types of Ti-6Al-4V specimen (a). A 100 mm diameter disc used for bulk double cone specimens; allowed to "free" cool after current switch-off (solid line). A 20 mm shaped mould when allowed to "free" cool after current switch-off (dotted line) with associated microstructure (b). A 20 mm shaped mould with "controlled" cool (dashed line) and associated microstructure (c).

Fig. 9: Micrographs of Ti-6Al-4V double truncated cone specimens produced via FAST at a dwell temperature of 1200°C. Showing microstructures from a shaped specimen (Shaped 1-4) at the locations outlined in the top left diagram; and a characteristic microstructure of the homogeneous bulk specimen (bottom right).

Fig. 10: Graphs of load-displacement curves during hot upset forging of Ti-6Al-4V double truncated cone specimens at 950°C and strain rates of 0.01 s^{-1}, 0.1 s^{-1}, and 1 s^{-}1. Bulk (solid lines) and shaped (dashed lines).

Fig. 11a: Light micrographs of the microstructural evolution with increasing strain from edge to centre of the double truncated cone specimens after forging at 950°C and 0.01 s^{-1}; produced from bulk (top) and via shaped FAST (bottom).

Fig. 11b: Light micrographs of the microstructural evolution with increasing strain from edge to centre of the double truncated cone specimens after forging at 950°C and 0.1 s^{-1}; produced from bulk (top) and via shaped FAST (bottom).

Fig. 11c: Light micrographs of the microstructural evolution with increasing strain from edge to centre of the double truncated cone specimens after forging at 950°C and 1 s^{-1}; produced from bulk (top) and via shaped FAST (bottom).

Fig. 12: Graphs comparing the load-displacement curves during the upset forging of double truncated cone specimens at 850°C (a), 950°C (b) and 1050°C (c) at strain rates of 0.01 s^{-1}, 0.1 s^{-1} and 1 s^{-1} (as labelled); from bulk FAST material (solid lines) against those obtained from DEFORM™ FE simulation (dotted lines).